# Supporting Information

# Controlling factors of oligomerization at the water surface: Why is isoprene such a unique VOC?

Shinnosuke Ishizuka,[a,b] Tomihide Fujii,[c] Akira Matsugi,[d] Yosuke Sakamoto,[c, e]* Tetsuya Hama,[a]* and Shinichi Enami[b]*

[a]Institute of Low Temperature Science, Hokkaido University, Sapporo 060-0819, Japan.

[b]National Institute for Environmental Studies, 16-2 Onogawa, Tsukuba 305-8506, Japan

[c]Graduate School of Global Environmental Studies, Kyoto University, Kyoto 606-8501, Japan

[d]Research Institute of Science for Safety and Sustainability, National Institute of Advanced Industrial Science and Technology, 16-1 Onogawa, Tsukuba 305-8569, Japan

[e]Graduate School of Human and Environmental Studies, Kyoto University, Kyoto 606-8316, Japan

*Authors to whom correspondence should be addressed: sakamoto.yosuke.7a@kyoto-u.ac.jp (YS), hama@lowtem.hokudai.ac.jp (TH), enami.shinichi@nies.go.jp (SE), phone: +81-29-850-2770

## SI Text

### Experimental Setup

Figure S1 shows a schematic diagram of the present experimental setup. An unsaturated hydrocarbon gas was introduced to the experimental chamber with buffer $N_2$ at a known flow rate (5–500 mL $min^{-1}$) through Teflon tube located just below the nebulizer. The vapor pressure values of 549, 634, 503, and 735 Torr for ISO, 1-p, 2-p, and 1,4-p, respectively, at 298 K were taken from literature reports.[1–3] The vapor pressure of 1,3-b was calculated to be 459 Torr at 298 K from the equilibrium vapor pressure of a hexane solution with a known 1,3-b content of 15 wt% assuming Raoult's law behavior: $P_{1,3-b} = P^{eq.}_{1,3-b} x_{1,3-b}$ where

$P_{1,3b}^{eq.}$ is the equilibrium vapor pressure of 1,3-b, and $x_{1,3-b}$ is the molar fraction of 1,3-b in the solution. The exposure values were calculated as following, $E_R = [R(g)] \times \tau$, where [R(g)] is the concentration of a reactant species and $\tau$ is the contact time, i.e., ~10 μs.

The pH-adjusted aqueous microjet was coaxial with a sheath through which the nebulizer gas $N_2$(g) was flowed at a high gas velocity. Upon hitting the microjet surface, a gas molecule can either become protonated by the microjet and adhere to its surface, or rebound into the gas-phase.[4–9] The concentration of the hydrocarbon in the reaction chamber is lower than its vapor pressure; the two quantities are related by a dilution factor that can be calculated from the ratio of carrier gas (5–500 mL $min^{-1}$) to drying gas flow rate (12 L $min^{-1}$).

The carbocation products we observed were formed when the gaseous hydrocarbon/$N_2$ collided with the intact aqueous microjets as they emerged from the grounded nozzle, i.e., before the microjets were broken up by the nebulizer gas. The possibility that the species we monitored were produced by the reaction of the gases with the small, highly concentrated, high surface-to-volume droplets formed by Coulomb explosions[7,8] was excluded based on previous experimental evidences[9–11] and Figure S3 where we newly studied how product mass signal distributions change as a function of the distance of the hydrocarbon gas inlet position from the nebulizer. Signal intensities of larger oligomers ($ISO_{n\geq3}H^+$) slightly decrease by injecting the ISO gas 13 mm and 24 mm downward relative to the standard position of the gas injector along the microjet direction (Fig. S3). Note that if the observed products were generated by the reaction of ISO(g) with such nanodroplets or gas-phase ions, we should have observed the *increase* of these signals. The observed slight decrease of larger oligomer species is consistent with the smaller concentration of ISO(g) at the region close to initial microjets caused by the lower injector position. The production of larger oligomers decreased while that of smaller oligomers $(ISO)_nH^+$ (n = 1, 2) instead slightly increased is

consistent with the result of Figure S2. Thus, these experiments support that the observed oligomers are indeed formed at the surface of intact microjets. It is also emphasized that the polarization of the initial microjets does not affect the observed phenomena as demonstrated before.[9,10,12,13] The absence of any signals corresponding to protonated products in the mass spectra of 1 mM ISO dissolved in a water:acetonitrile (vol:vol = 1:1) solution at $1.9 < pH < 4.3$,[14] 1 mM α-pinene dissolved in a water:acetonitrile (1:1) solution at $1.1 < pH < 6.0$, or in a water:methanol (1:1) solution at $1.5 < pH < 7.5$[15] was convincing evidence that the observed reactions occur at the gas side rather than the bulk side of the interface. A key feature of our instrument is that the microjet spraying from the nozzle source is orthogonal to the polarized inlet to the mass spectrometer. The initial microjets containing droplets ($D_0 > 1\mu m$) are transformed into thin-films and rims by nebulizer $N_2$ gas, where only the thin-films produce smaller droplets, that ultimately emit gas-phase ions.[4,16] Gas-phase ions are finally sorted out and detected by the online quadrupole mass spectrometer. Further experimental details can be found in previous publications.[9,12,17,18]

**Protonation of ISO at the air–water interface**

The cationic oligomerization of ISO is initiated by the protonation of ISO at the air–water interface. There are four possible reaction sites for the protonation of ISO (see Scheme S1), which produce two types of primary carbocations (B and C), a secondary carbocation (D), and a tertiary carbocation (A). Considering the thermodynamic stability of carbocations (primary < secondary < tertiary), tertiary carbocation formation (A) is expected to be preferred. It is noted that the carbocations could undergo a rapid isomerization via intramolecular H transfers and/or structural rearrangements before undergoing propagation reactions with neutral ISO molecules. For example, a primary carbocation may undergo rapid isomerization to a more stable tertiary carbocation via intramolecular hydrogen atom transfer reaction (e.g., B in Scheme S1).

**Quantum chemical calculations of the carbocationic reactions**

The initial proton transfer reactions and the dimerization of ISO and 1-p were investigated using quantum chemical calculations at the CBS-QB3//ωB97X-D/6-311++G(d,p) level of theory[20-22] using the program Gaussian 09.[23] The zero-point energy corrected ground-state energies are reported here.

Figure S5 shows the energy diagrams for the initial $H^+$ addition to the carbon sites 1 and 4 of ISO (the reactions forming A and D in Scheme S1, respectively) with $H_3O^+$, $H_5O_2^+$, and $H_7O_4^+$ as the proton donors. The addition of $H^+$ to the 2- and 3-carbon sites was also investigated, but the corresponding carbocations (B and C in Scheme S1) were found to be unstable; no local minima were found by geometry optimizations at the ωB97X-D/6-311++G(d,p) level of theory. Therefore, the $H^+$ addition reactions primarily occurred at the 1- and 4-carbon sites. The proton transfer in the reactions of ISO with $H_3O^+$ proceeded without a barrier to produce weakly bound complexes of A (or D) (denoted as 1H-ISO$^+$ or 4H-ISO$^+$ in Figure S1) and $H_2O$, which could dissociate directly to A (or D) and $H_2O$. In contrast, the reactions of ISO with $H_5O_2^+$ and $H_7O_3^+$ first formed the wells of the two reactants (shown as ISO-$(H_2O)_mH^+$), which could then isomerize via intramolecular proton transfer transition states (P.T. TS) to produce the complexes of A (or D) with $H_4O_2$ and $H_6O_3$. These post-proton-transfer complexes could easily isomerize to structures with different water orientations, as indicated with dashed lines in the figure (no searches for transition states were carried out for these isomerization reactions). These complexes can dissociate to the carbocations and $(H_2O)_m$, or to the alcohols and $(H_2O)_{m-1}H^+$. Although the formation of alcohols from ISOH$^+$ and $(H_2O)_m$ was endothermic for $m \leq 2$, it became almost thermoneutral or exothermic for $m \geq 3$. The $H^+$ addition reaction for 1-p was also investigated, as shown in Figure S6. The energy diagram for 1-p is qualitatively similar to that of ISO; however, their reaction energies were markedly different, as 1-p has smaller proton affinity than ISO.

To elucidate the chain propagation pathway, the dimerization of 1H-$ISO^+$ (A in Scheme S1) and 4H-$ISO^+$ (D in Scheme S1) were also studied.

$$ISOH^+(g) + ISO\ (g) \rightarrow (ISO)_2H^+(g) \qquad (RS1)$$

The calculations showed that the dimerization of ISO proceeds without a barrier for all ISO addition sites (Table S1). We found that the 1,4-addition of 1H-$ISO^+$ (4-1 in Table S1) was the more probable of the two pathways. The dimerization of 1-p was also barrierless and highly exothermic in the gas phase.

The proton affinities of the molecules including other acyclic compounds (see Table 1 in main text) at 298 K were calculated at the same level of theory using the rigid-rotor and harmonic-oscillator approximations.

**Estimation of reaction efficiency of chain-propagation**

We roughly estimate the reaction efficiency to account for the observed chain-propagation yields up to the n = 10 oligomers. Here the reaction efficiency is defined as the ratio of the number of successful chain-propagation to all collisions of ISO(g) on activated carbocations on the surface. By assuming collision-controlled growth based on an Eley-Rideal mechanism, in which ISO(g) is directly supplied from gas phase to an activated carbocation on the water surface, and the maximum [ISO(g)] conditions, ISO(g) gases hit on the water surface with a flux $1.69 \times 10^{27}$ $m^{-2}$ $s^{-1}$. The number of ISO(g) gases collide with an activated carbocation $(ISO)_nH^+$ on the $1 \times 10^{-18}$ $m^2$ area of the water surface in the present exposure time $\sim 10 \times 10^{-6}$ s is derived to be $1.7 \times 10^4$ molecules. Here we assumed that the area of ~1 $nm^2$ as a distance where $(ISO)_nH^+$ react with a neutral ISO at the water surface. Furthermore, since the reaction efficiency of the observed chain-propagation would depend on neutral monomer's (i.e., ISO) structure rather than terminal molecular structures of active carbocation,[19] we

assumed the chain-propagation for $(ISO)_nH^+$ is independent of oligomer length. Then, the reaction efficiency of the chain-propagation to account for the observed $(ISO)_{10}H^+$ formation is estimated to be $\geq 5.9 \times 10^{-4}$. The introduced ISO gas with buffer $N_2$ (0.5 L $min^{-1}$ for $(ISO)_{10}H^+$ formation) will be diluted by drying $N_2$ (12 L $min^{-1}$) up to ~24 times. This condition yields the reaction efficiency $\geq 1.4 \times 10^{-2}$. Thus, it could be concluded that the $(ISO)_{10}H^+$ formation during the present ISO(g) exposure is reasonable. These values of reaction efficiencies are considerably larger than the reported uptake coefficient of ISO(g) on acidic surfaces, $\sim 10^{-6}$,[14] implying that the initial uptake via proton transfer between $H_3O^+(H_2O)_m$ ($m < 5$) and ISO(g) is a rate-determining step in the observed oligomerization process.

**References for Supporting Information**


(1) Scott, D. W.; Waddington, G. Vapor Pressure of Cis-2-Pentene, Trans-2-Pentene and 3-Methyl-1-Butene. *J. Am. Chem. Soc.* **1950**, *72* (9), 4310–4311.

(2) Linstrom, P. J.; Mallard, W. G. *NIST Chemistry webBook, NIST Standard Reference Database Number 69*; 2014.

(3) Letcher, T. M.; Marsicano, F. Vapour Pressures and Densities of Some Unsaturated C6 Acyclic and Cyclic Hydrocarbons between 300 and 320 K. *J. Chem. Thermodyn.* **1974**, *6* (5), 509–514.

(4) Enami, S.; Colussi, A. J. Long-Range Specific Ion-Ion Interactions in Hydrogen-Bonded Liquid Films. *J. Chem. Phys.* **2013**, *138* (18), 2–7.

(5) Dempsey, L. P.; Brastad, S. M.; Nathanson, G. M. Interfacial Acid Dissociation and Proton Exchange Following Collisions of DCl with Salty Glycerol and Salty Water. *J. Phys. Chem. Lett.* **2011**, *2* (6), 622–627.

(6) Davidovits, P.; Kolb, C. E.; Williams, L. R.; Jayne, J. T.; Worsnop, D. R. Mass Accommodation and Chemical Reactions at Gas−Liquid Interfaces. *Chem. Rev.* **2006**, *106* (4), 1323–1354.

(7) Kebarle, P.; Peschke, M. On the Mechanisms by Which the Charged Droplets Produced by Electrospray Lead to Gas Phase Ions. *Anal. Chim. Acta* **2000**, *406* (1),

11–35.

(8) Kebarle, P. A Brief Overview of the Present Status of the Mechanisms Involved in Electrospray Mass Spectrometry. *J. Mass Spectrom.* **2000**, *35* (7), 804–817.

(9) Enami, S.; Hoffmann, M. R.; Colussi, A. J. Molecular Control of Reactive Gas Uptake "on Water." *J. Phys. Chem. A* **2010**, *114* (18), 5817–5822.

(10) Enami, S.; Vecitis, C. D.; Cheng, J.; Hoffmann, M. R.; Colussi, A. J. Electrospray Mass Spectrometric Detection of Products and Short-Lived Intermediates in Aqueous Aerosol Microdroplets Exposed to a Reactive Gas. *J. Phys. Chem. A* **2007**, *111* (50), 13032–13037.

(11) Enami, S.; Sakamoto, Y.; Colussi, A. J. Fenton Chemistry at Aqueous Interfaces. *Proc. Natl. Acad. Sci.* **2014**, *111* (2), 623–628.

(12) Enami, S.; Hoffmann, M. R.; Colussi, A. J. Proton Availability at the Air/water Interface. *J. Phys. Chem. Lett.* **2010**, *1* (10), 1599–1604.

(13) Mishra, H.; Enami, S.; Nielsen, R. J.; Stewart, L. A.; Hoffmann, M. R.; Goddard, W. A.; Colussi, A. J. Bronsted Basicity of the Air-Water Interface. *Proc. Natl. Acad. Sci.* **2012**, *109* (46), 18679–18683.

(14) Enami, S.; Mishra, H.; Hoffmann, M. R.; Colussi, A. J. Protonation and Oligomerization of Gaseous Isoprene on Mildly Acidic Surfaces: Implications for Atmospheric Chemistry. *J. Phys. Chem. A* **2012**, *116* (24), 6027–6032.

(15) Enami, S.; Hoffmann, M. R.; Colussi, A. J. Dry Deposition of Biogenic Terpenes via Cationic Oligomerization on Environmental Aqueous Surfaces. *J. Phys. Chem. Lett.* **2012**, *3* (21), 3102–3108.

(16) Enami, S.; Fujii, T.; Sakamoto, Y.; Hama, T.; Kajii, Y. Carboxylate Ion Availability at the Air–Water Interface. *J. Phys. Chem. A* **2016**, *120* (46), 9224–9234.

(17) Enami, S.; Stewart, L. A.; Hoffmann, M. R.; Colussi, A. J. Superacid Chemistry on Mildly Acidic Water. *J. Phys. Chem. Lett.* **2010**, *1* (24), 3488–3493.

(18) Enami, S.; Hoffmann, M. R.; Colussi, A. J. Extensive H-Atom Abstraction from Benzoate by OH-Radicals at the Air–water Interface. *Phys. Chem. Chem. Phys.* **2016**, *18* (46), 31505–31512.

(19) Matyjashewski, K. *Cationic Polymerizations: Mechanisms, Synthesis and Applications*; 1996; Vol. 25.

(20) Montgomery Jr., J. A.; Frisch, M. J.; Ochterski, J. W.; Petersson, G. A. A Complete Basis Set Model Chemistry. VI. Use of Density Functional Geometries and Frequencies. *J. Chem. Phys.* **1999**, *110* (6), 2822–2827.

(21) Chai, J.-D.; Head-Gordon, M. Long-Range Corrected Hybrid Density Functionals with Damped Atom-Atom Dispersion Corrections. *Phys. Chem. Chem. Phys.* **2008**, *10* (44), 6615–6620.

(22) Matsugi, A.; Shiina, H. Kinetics of Hydrogen Abstraction Reactions from Fluoromethanes and Fluoroethanes. *Bull. Chem. Soc. Jpn.* **2014**, *87* (8), 890–901.

(23) Frisch, M. J.; Trucks, G. W.; Schlegel, H. B.; Scuseria, G. E.; Robb, M. A.; Cheeseman, J. R.; Scalmani, G.; Barone, V.; Mennucci, B.; Petersson, G. A.; et al. *Gaussian 09*, Revision C.01, Gaussian, Inc.: Wallingford CT, 2010.

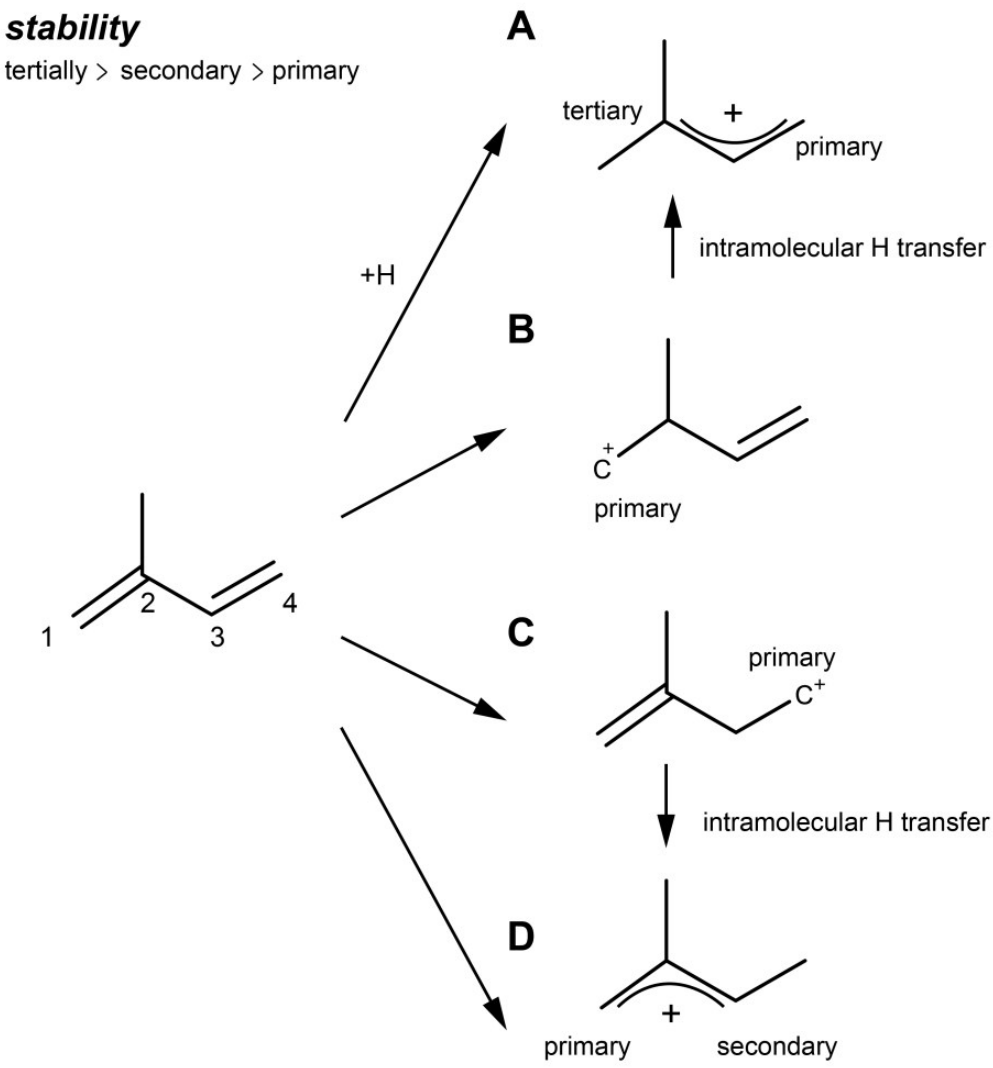


**Scheme S1.** Schematic illustration of protonated ISO monomer structures. A is the most stable form of $ISOH^+$, and has a resonance with a tertiary and primary carbocation. B is a primary carbocation that can isomerize to A via intramolecular hydrogen transfer. C is the most unstable form of $ISOH^+$, having only a primary carbocation form. D is a secondary stable $ISOH^+$ with a resonance between a secondary and primary carbocation.

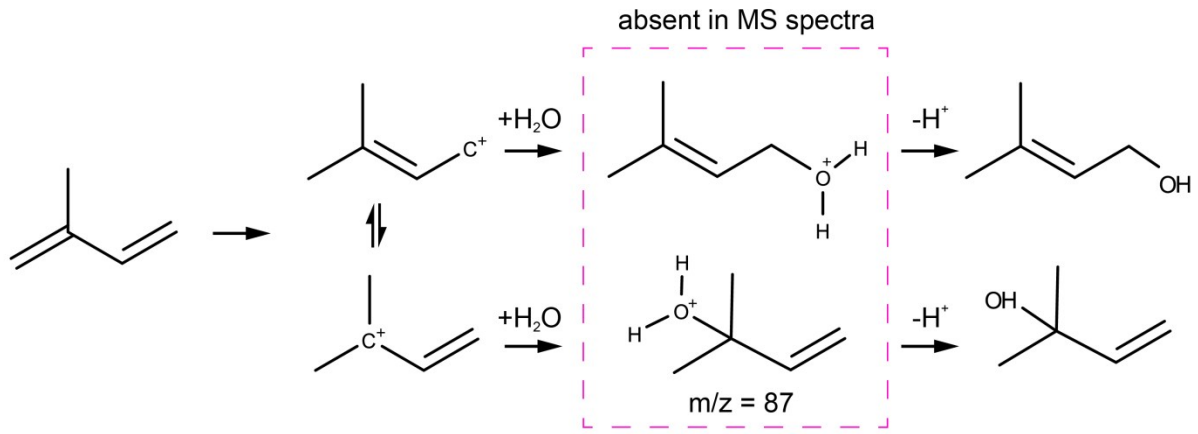


**Scheme S2.** A possible pathway of the formation of oxocarbenium ions from the hydration of carbocations.

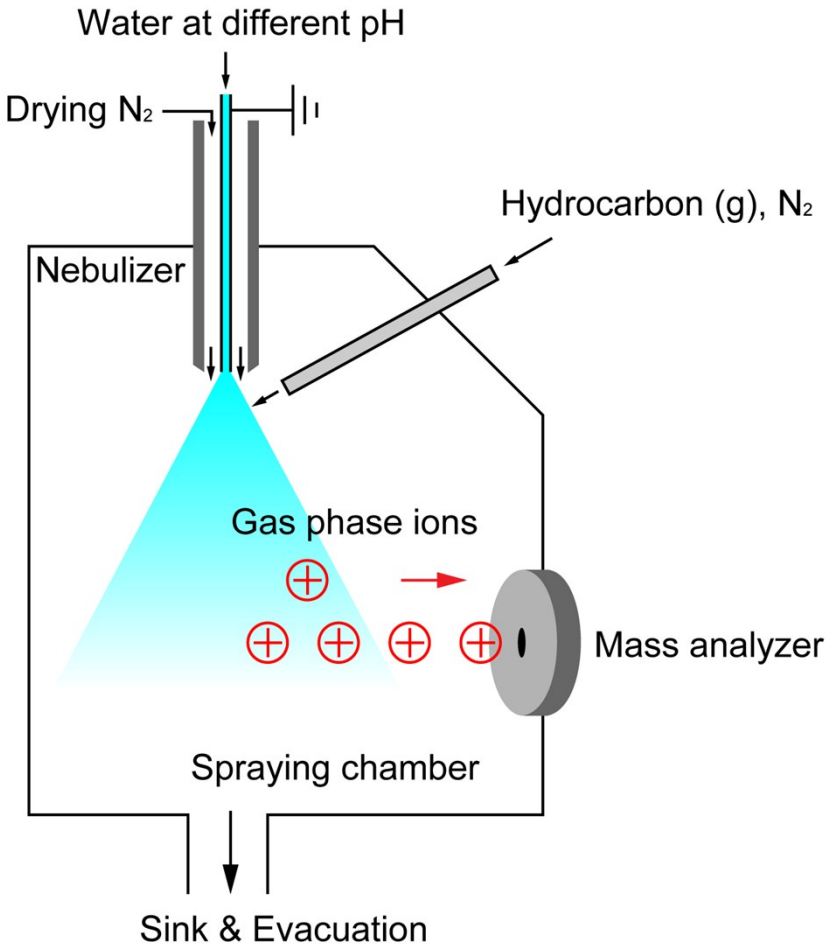


**Figure S1.** Schematic diagram of the microjet experimental system.

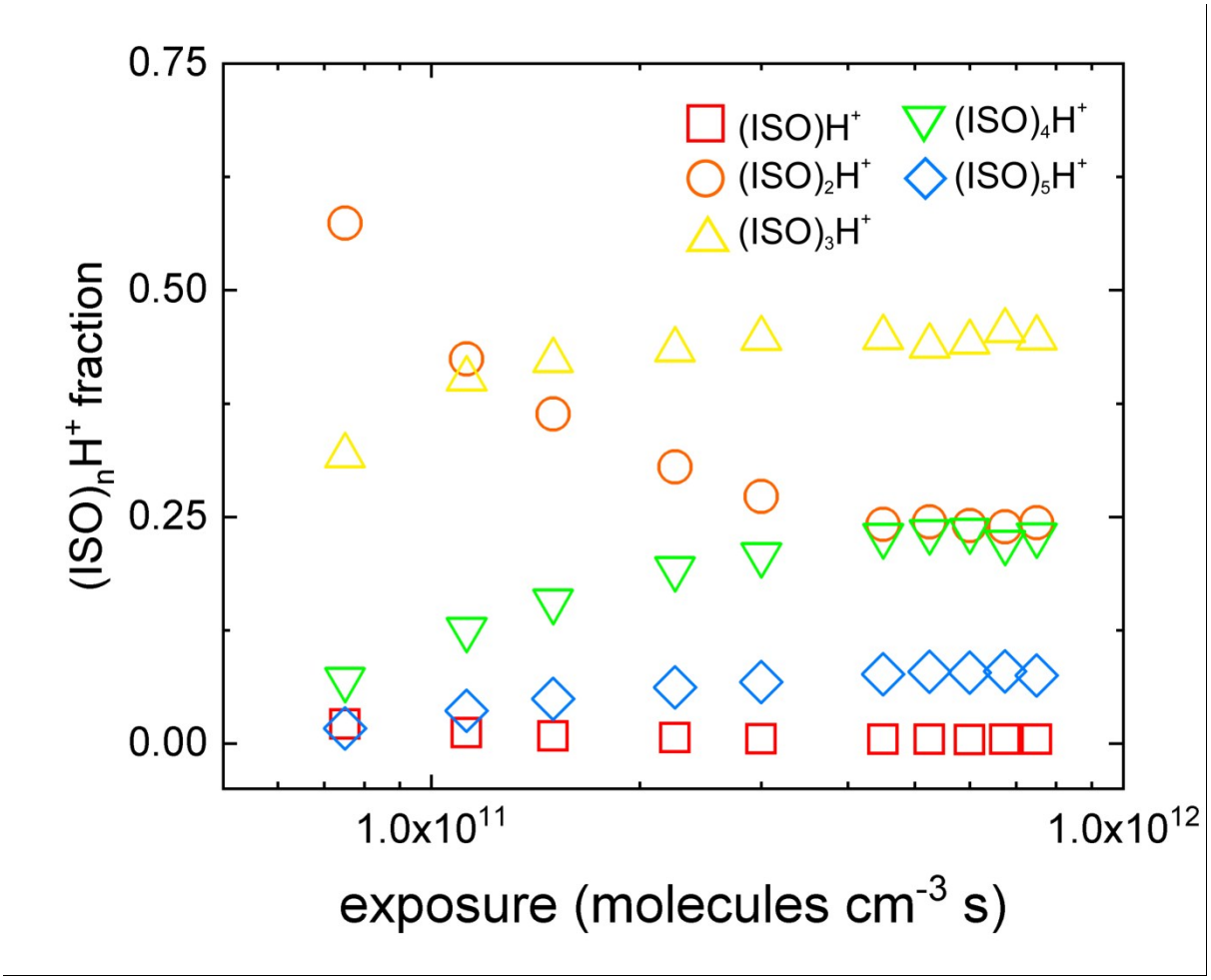


**Figure S2.** Relative signal intensities of $(ISO)_nH^+$ (n = 1-5) to the sum of the signals as a function of the exposure, in experiments performed on $H_2O$ microjets at pH = 1.98.

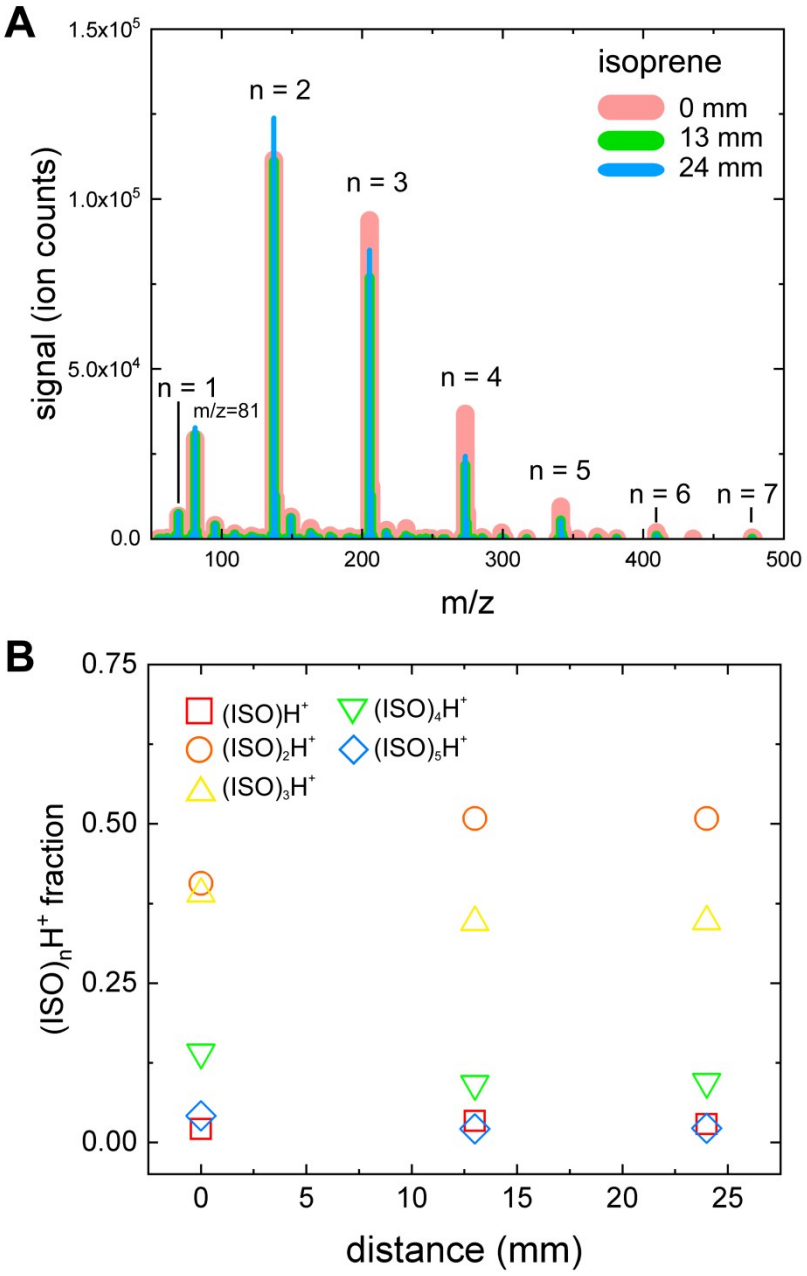


**Figure S3.** (A) Positive ion mass spectra measured with ISO (g) exposure at $E = 3 \times 10^{11}$ molecules cm$^{-3}$ s obtained from different vertical gas-injection distance between the position of reactive gas inlet and the nebulizer: 0 mm (pink), 13 mm (green) and 24 mm (blue). (B) Relative signal intensities of $(ISO)_nH^+$ (n = 1-5) to the sum of the $(ISO)_nH^+$ signals as a function of the distance of ISO(g) injection from the nebulizer.

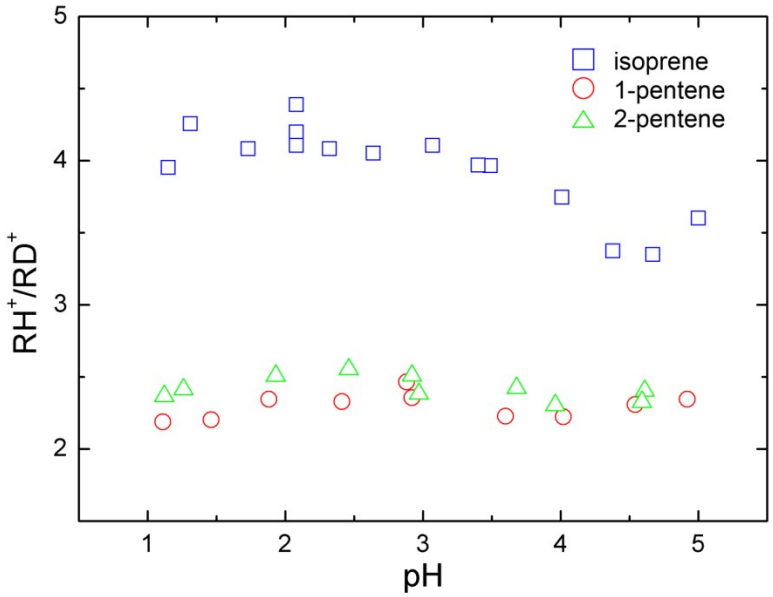


**Figure S4.** Ratios of $RH^+/RD^+$ (monomers) as a function of bulk pH, in experiments performed on $H_2O$:$D_2O$ (1:1 = vol:vol) microjets exposed to isoprene (squares), 1-pentene (circles) or 2-pentene (triangles), under $E \approx 3 \times 10^{11}$ molecules $cm^{-3}$ s. All experiments were performed in 1 atm $N_2$(g) at 298 K. The contributions of the $^{13}C$ satellites of $RH^+$ signals to the $RD^+$ signal intensities were subtracted in all cases.

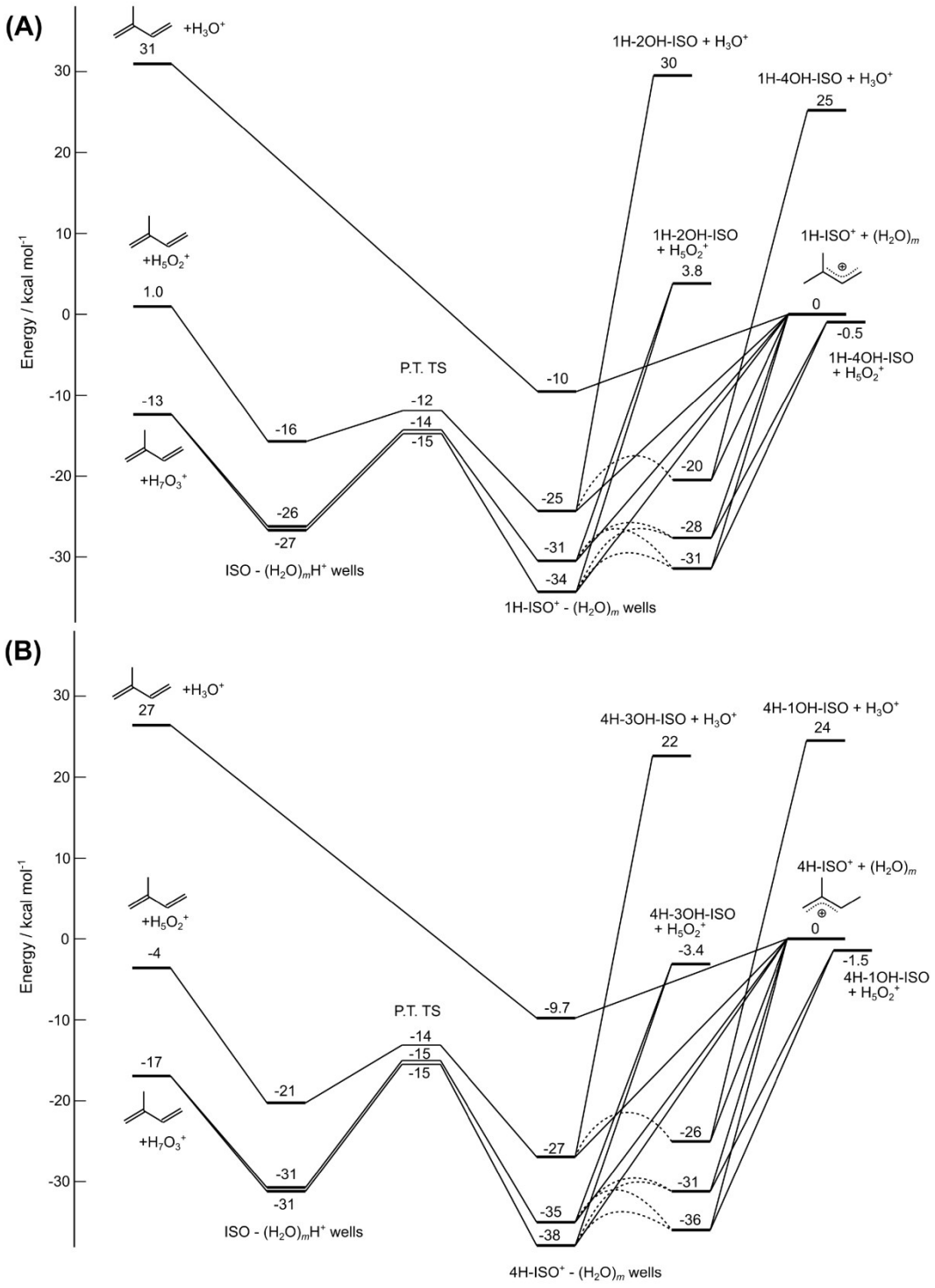


**Figure S5.** Schematic of ISO + $(H_2O)_mH^+$ energy surfaces. Protonation reactions resulting in (A) 1H-ISO$^+$ and (B) 4H-ISO$^+$ formation are shown.

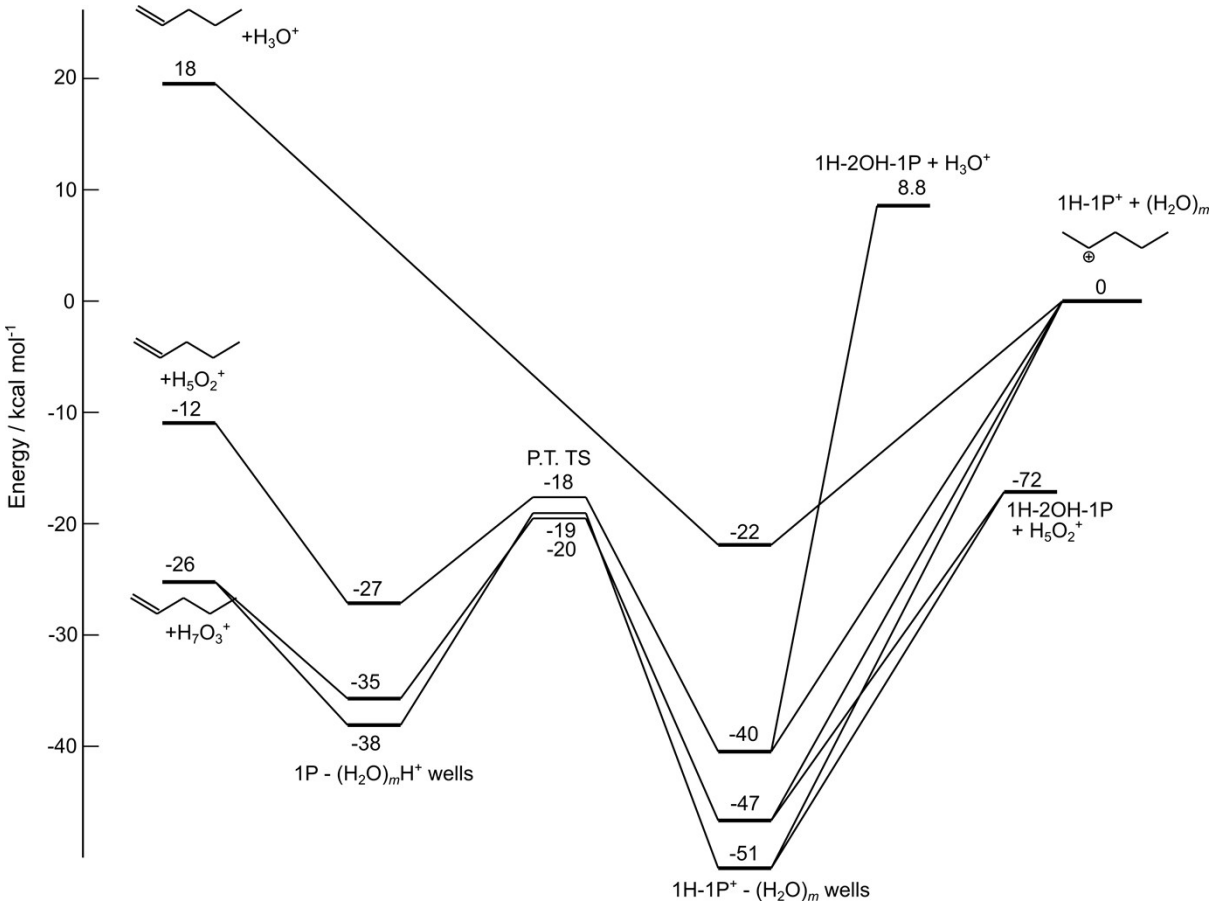


**Figure S6.** A schematic of 1-p + $(H_2O)_mH^+$ energy surfaces.

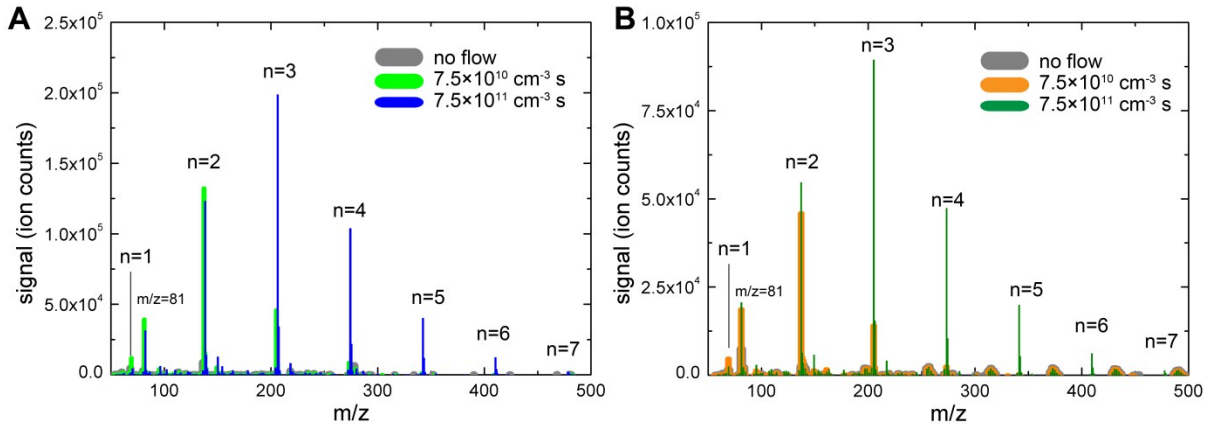


**Figure S7.** Positive ion mass spectra of (A) water and (B) 10 mM NaCl water microjets at pH = 3.0 with/without ISO(g) exposure. The m/z values of $(ISO)_nH^+$ (n = 1–7) were 69.1, 137.1, 205.2, 273.3, 341.3, 409.4, and 477.5, respectively.

**Table S1.** Energy difference between the reactants and products for the dimerization of 1H-ISO$^+$, 4H-ISO$^+$, and 1H-1-p$^+$.

| protonation | addition | kcal mol$^{-1}$ |
|---|---|---|
| 1H-ISO$^+$ | 2-1 | -23 |
| | 2-4 | -18 |
| | 4-1 | -27 |
| | 4-4 | -20 |
| 4H-ISO$^+$ | 1-1 | -26 |
| | 1-4 | -20 |
| | 3-1 | -25 |
| | 3-4 | -19 |
| 1H-1p$^+$ | 2-1 | -33 |